

Cluster folding analysis of $^{20}\text{Ne} + ^{16}\text{O}$ elastic transfer

Sh. Hamada,¹ N. Keeley,² K. W. Kemper,^{3,4} and K. Rusek⁴

¹*Faculty of Science, Tanta University, Tanta, Egypt*

²*National Centre for Nuclear Research, ulica Andrzeja Soltana 7, 05-400 Otwock, Poland*

³*Department of Physics, Florida State University, Tallahassee, Florida 32306, USA*

⁴*Heavy Ion Laboratory, University of Warsaw, ulica Pasteura 5a, 02-093 Warsaw, Poland*



(Received 19 October 2017; revised manuscript received 25 April 2018; published 21 May 2018)

The available experimental data for the $^{20}\text{Ne} + ^{16}\text{O}$ system in the energy range where the effect of α -cluster transfer is well observed are reanalyzed using the cluster folding model. The cluster folding potential, which includes both real and imaginary terms, reproduces the data at forward angles and the inclusion of the $^{16}\text{O}(^{20}\text{Ne}, ^{16}\text{O})^{20}\text{Ne}$ elastic transfer process provides a satisfactory description of the backward angles. The spectroscopic factor for the $^{20}\text{Ne} \rightarrow ^{16}\text{O} + \alpha$ overlap was extracted and compared with other values from the literature. The present results suggest that the $(^{20}\text{Ne}, ^{16}\text{O})$ reaction might be an alternative means of exploring the α -particle structure of nuclei.

DOI: [10.1103/PhysRevC.97.054609](https://doi.org/10.1103/PhysRevC.97.054609)

I. INTRODUCTION

Systems where the projectile and target differ by a single nucleon or cluster of nucleons, such as an α particle, may exhibit the phenomenon known as “elastic transfer” whereby the excess nucleon or cluster is exchanged between the two identical cores to leave an exit channel that is experimentally indistinguishable from conventional elastic scattering. The interference between the amplitudes for the two processes often gives rise to a significant increase in the elastic scattering cross section at backward angles. Conventional optical model calculations are frequently unable to reproduce the experimental data over the whole angular range when such transfer phenomena are present, consequently different methods such as the distorted wave Born approximation (DWBA), coupled channels Born approximation (CCBA), and coupled reaction channels (CRC) are employed to include explicitly the exchange process in the analysis.

In addition to its interest from the reaction mechanism point of view elastic transfer has much to recommend it as a means of extracting spectroscopic factors. Since the entrance and exit channels are identical, only one overlap function and one distorting potential are required—the projectile and target overlaps are identical, as are the entrance and exit channels—thus halving two of the main sources of model dependence of “empirical” spectroscopic factors. Absolute α -particle spectroscopic factors extracted from analyses of transfer data are notoriously reaction and model dependent. Two of the most popular α -transfer reactions, $(^6\text{Li}, d)$ and $(^7\text{Li}, t)$, are both complicated by the low breakup thresholds of the projectile (and ejectile in the case of ^6Li). One possible α -transfer reaction that avoids this problem, the $(^{20}\text{Ne}, ^{16}\text{O})$ reaction, has been little exploited, presumably due to the unavailability of Ne beams from tandem Van de Graaff accelerators. However, to employ this reaction to extract reliable absolute α spectroscopic factors a well-defined $(^{20}\text{Ne} | ^{16}\text{O} + \alpha)$ overlap is required. Due to the peculiarities

outlined above, the $^{16}\text{O}(^{20}\text{Ne}, ^{16}\text{O})^{20}\text{Ne}$ elastic transfer reaction is a promising means of obtaining this overlap.

There are several measurements and studies of this reaction in the literature. In Ref. [1] angular distributions were measured for the $^{20}\text{Ne} + ^{16}\text{O}$ scattering to the ground and 2_1^+ and 4_1^+ excited states of ^{20}Ne at an incident ^{20}Ne energy of 50 MeV and analyzed using both the optical model (OM) and CRC formalisms. In Ref. [2] excitation functions and angular distributions for $^{16}\text{O} + ^{20}\text{Ne}$ elastic scattering were measured in the energy ranges $E_{\text{c.m.}} = 9\text{--}30$ MeV and $E_{\text{c.m.}} = 14.2\text{--}24.7$ MeV, respectively and the observed increases in the cross sections at large angles were studied using both optical model plus resonance and DWBA α -exchange frameworks. Kondō *et al.* [3–5] studied the gross structures observed in $^{20}\text{Ne} + ^{16}\text{O}$ elastic scattering and the $^{20}\text{Ne}(^{16}\text{O}, ^{12}\text{C})^{24}\text{Mg}_{\text{g.s.}}$ reaction in the energy range $E_{\text{c.m.}} = 22.8\text{--}38.6$ MeV using potentials including a parity dependent real part and angular momentum (J) dependent absorptive part and reported that the experimental angular distributions could be well described by making the optical potential surface transparent. In a later work [6] they found that the parity dependent term in the real potential well simulated the effect of the α -particle elastic transfer. In Ref. [7] the gross structure observed in the $^{20}\text{Ne} + ^{16}\text{O}$ angular distributions was analyzed using a deep optical potential. Burtebayev *et al.* [8] also tried to reproduce the experimental data for $^{20}\text{Ne} + ^{16}\text{O}$ elastic scattering at $E_{\text{lab}} = 50$ MeV using a deep real potential plus Woods-Saxon surface and volume imaginary potentials. All these previous studies constructed the interaction potential on a purely phenomenological basis and until recently there were no theoretical calculations for $^{20}\text{Ne} + ^{16}\text{O}$ angular distributions on a microscopic or semimicroscopic basis.

Yang and Li [9] studied the $^{20}\text{Ne} + ^{16}\text{O}$ elastic scattering in the energy range $E_{\text{c.m.}} = 24.5\text{--}35.5$ MeV using a real potential obtained from a folding model based on a 4α model of ^{16}O

and an $\alpha + {}^{16}\text{O}$ model of ${}^{20}\text{Ne}$ and an empirical imaginary part consisting of either a standard volume Woods-Saxon term or volume Woods-Saxon plus surface Woods-Saxon derivative terms. The experimental data at these energies show a significant rise in differential cross section at backward angles, often assigned to α -cluster “elastic transfer.” However, the authors were able to reproduce the experimental data over the whole angular range without either explicitly including the α -cluster exchange or introducing parity and/or angular momentum dependence, thus demonstrating that the marked increase in the ${}^{20}\text{Ne} + {}^{16}\text{O}$ elastic scattering cross section in the backward hemisphere can also be described within the conventional optical model picture with a deep real potential derived from an α -cluster picture of the structure of ${}^{20}\text{Ne}$ and a long-range imaginary potential.

In the current work we develop a more microscopic analysis of the ${}^{20}\text{Ne} + {}^{16}\text{O}$ elastic scattering based on a cluster folding (CF) potential and the explicit inclusion of α -cluster exchange between the two ${}^{16}\text{O}$ cores, which we use to extract a spectroscopic factor (SF) for the ${}^{20}\text{Ne} \rightarrow {}^{16}\text{O} + \alpha$ configuration. Previous work, reviewed briefly above, has shown that the extent to which the backward angle rise in the experimental elastic scattering angular distributions may be attributed to the elastic transfer process is particularly dependent on the choice of both the real and imaginary parts of the optical potential. The Watanabe-type folding procedure employed in the ${}^{16}\text{O} + \alpha$ cluster model yields the imaginary part of the optical potential as well as the real part, unlike previous semimicroscopic analyses. Therefore, we hope to minimize what are probably the largest sources of the model dependence of the extracted SF in this system, the choice of distorting optical potential and $\alpha + {}^{16}\text{O}$ binding potential, by a self-consistent approach. We give results for analyses where the normalization factors of the real and imaginary parts of the CF optical potential were tuned to give the best agreement with the elastic scattering data in the forward hemisphere ($\theta_{\text{c.m.}} < 90^\circ$) at each energy and where they were both held fixed at 1.0 for all data sets. We further make the assumption that DWBA is an adequate model to describe the transfer process and that any two-step transfer paths, for example inelastic excitation of the ${}^{20}\text{Ne}$ followed by transfer of an α particle, will affect the phase of the backward angle oscillations in the elastic scattering cross section rather than its overall magnitude, thus enabling a reliable value for the SF to be extracted. Consistent results for the ${}^{20}\text{Ne} \rightarrow {}^{16}\text{O} + \alpha$ SF extracted from several data sets provide *a posteriori* justification for these assumptions.

The paper is organized as follows. In Sec. II the CF potential for the ${}^{20}\text{Ne} + {}^{16}\text{O}$ system is described, together with the DWBA calculations of the ${}^{16}\text{O}({}^{20}\text{Ne}, {}^{16}\text{O}){}^{20}\text{Ne}$ elastic transfer. Section III is devoted to a discussion of the results and our conclusions are given in Sec. IV.

II. CALCULATIONS

A. Cluster folding potential for the ${}^{20}\text{Ne} + {}^{16}\text{O}$ system

Motivated by the well-known $\alpha + {}^{16}\text{O}$ cluster structure of ${}^{20}\text{Ne}$, existing experimental data [2,3] for ${}^{20}\text{Ne} + {}^{16}\text{O}$ elastic scattering were analyzed using a cluster folding (CF) model

TABLE I. Parameters of the imaginary parts of the $\alpha + {}^{16}\text{O}$ and ${}^{16}\text{O} + {}^{16}\text{O}$ potentials used as input to the ${}^{20}\text{Ne} + {}^{16}\text{O}$ CF potential. Radii $R_w = r_w \times (a^{1/3} + 16^{1/3})$ fm where $a = 0$ or 16 for an α or ${}^{16}\text{O}$ projectile, respectively. The real parts were calculated using the double-folding procedure.

System	W (MeV)	r_w (fm)	a_w (fm)
$\alpha + {}^{16}\text{O}$	7.27	1.139	0.15
${}^{16}\text{O} + {}^{16}\text{O}$	7.012	1.414	0.302

potential as a basis. The data considered are in the energy range $E_{\text{c.m.}} = 24.5\text{--}35.5$ MeV where the effect of α -cluster exchange between the core nuclei and its role in producing the backward angle rise in the cross section are well observed. All reaction calculations were performed using the code FRESKO [10].

The basic ingredients needed to calculate a CF potential for the ${}^{20}\text{Ne} + {}^{16}\text{O}$ system are an $\alpha + {}^{16}\text{O}$ binding potential, required to calculate the wave function for the relative motion of the α and ${}^{16}\text{O}$ in ${}^{20}\text{Ne}$, and $\alpha + {}^{16}\text{O}$ and ${}^{16}\text{O} + {}^{16}\text{O}$ optical potentials, obtained by fitting the respective elastic scattering data for the same value of E/A as the ${}^{20}\text{Ne}$ data of interest. The CF ${}^{20}\text{Ne} + {}^{16}\text{O}$ optical potential is then obtained by Watanabe-type folding [11] of the $\alpha + {}^{16}\text{O}$ and ${}^{16}\text{O} + {}^{16}\text{O}$ potentials over the $\alpha + {}^{16}\text{O}$ cluster wave function of ${}^{20}\text{Ne}$. In this work, the $\alpha + {}^{16}\text{O}$ binding potential was taken from Ref. [12] and the $\alpha + {}^{16}\text{O}$ and ${}^{16}\text{O} + {}^{16}\text{O}$ optical potentials were obtained by fitting appropriate elastic scattering data [13,14]. The real parts of both these potentials were calculated using the double-folding method [15] with the density-dependent BDM3Y1 nucleon-nucleon effective interaction [16]. The nuclear matter density distributions for the α particle and ${}^{16}\text{O}$ were taken from Refs. [15] and [17] and were of simple and modified Gaussian forms, respectively. No normalization of these potentials was necessary in order to fit the respective data. The imaginary parts were purely phenomenological and of conventional Woods-Saxon volume form with parameters given in Table I. Both the real and imaginary parts of these potentials were then folded over the cluster wave function to produce the ${}^{20}\text{Ne} + {}^{16}\text{O}$ CF potential.

The CF potential calculated in this way was then used to fit the experimental ${}^{20}\text{Ne} + {}^{16}\text{O}$ elastic scattering angular distributions in the forward hemisphere ($\theta_{\text{c.m.}} < 90^\circ$) only, with two adjustable parameters, N_R and N_I , the normalization factors of the real and imaginary parts of the CF potential. The full optical potential thus had the following form:

$$U(r) = V_C(r) - N_R V_{\text{CF}}(r) - i N_I W_{\text{CF}}(r), \quad (1)$$

where $V_C(r)$ is the usual Coulomb potential with a radius of $R_C = 1.3 \times (16^{1/3} + 20^{1/3})$ fm. The optimal values of N_R and N_I at each energy were obtained by minimizing χ^2 using SFRESKO, the searching version of FRESKO. The best fit values are listed in Table II.

The mean values of N_R and N_I are 0.986 ± 0.006 and 0.986 ± 0.019 respectively, the individual values being only weakly dependent on energy, thus providing *a posteriori* justification for the CF model as a basis for the potential scattering in this system. The quoted uncertainties are the

TABLE II. Best fit N_R and N_I values for the $^{20}\text{Ne} + ^{16}\text{O}$ elastic scattering data at the different energies studied in this work, together with real and imaginary volume integrals and spectroscopic factors (C^2S) extracted from the DWBA analysis; see text for details. Note that the χ^2/N values refer to $\theta_{c.m.} < 90^\circ$ for the optical model calculations and the full angular range for the DWBA calculations.

$E_{c.m.}$ (MeV)	Model	N_R	N_I	C^2S	σ_R (mb)	J_V (MeV fm 3)	J_W (MeV fm 3)	χ^2/N
24.5	OM CF	0.973	0.908		1079	425.75	37.2	4.4
	DWBA			0.64 ± 0.08				38.5
24.7	OM CF	1.002	1.007		1097	438.43	41.3	5.9
	DWBA			0.44 ± 0.11				62.0
27.9	OM CF	1.006	1.027		1207	440.18	42.1	4.6
	DWBA			0.45 ± 0.08				32.4
28.2	OM CF	0.989	0.899		1207	432.75	36.9	5.4
	DWBA			0.53 ± 0.07				51.5
29.1	OM CF	1.008	1.055		1241	441.06	43.2	13.9
	DWBA			0.66 ± 0.09				34.6
31.7	OM CF	0.996	0.982		1298	435.81	40.25	9.1
	DWBA			0.46 ± 0.10				42.7
32.1	OM CF	0.97	1.026		1304	424.43	42.06	14.7
	DWBA			0.88 ± 0.13				35.4
33.0	OM CF	0.95	0.94		1312	415.68	38.53	18.7
	DWBA			0.40 ± 0.09				26.8
35.5	OM CF	0.98	1.03		1368	428.81	42.22	19.1
	DWBA			0.49 ± 0.09				73.5

standard deviations of the mean values, the so-called mean error. The optical model fits to the data are denoted in Figs. 1–3 by the dashed black curves. The description of the forward angle data is in general good, reflected in the relatively low χ^2/N values of Table II, although there is a tendency for the optical model calculations to be more structured than the data as $E_{c.m.}$ increases.

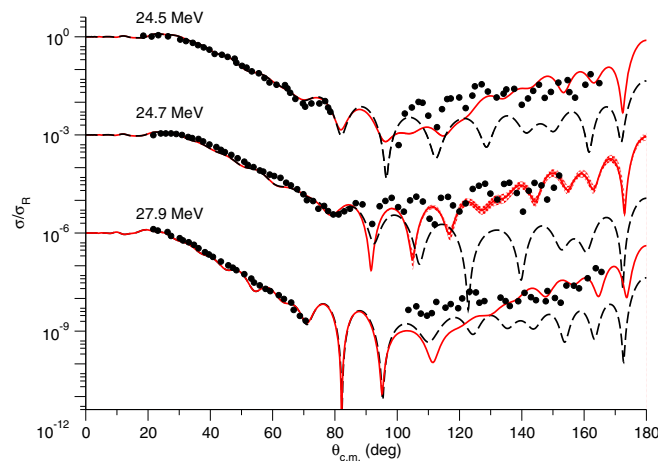


FIG. 1. Comparison between the data (solid black circles) and calculations for the $^{16}\text{O}(^{20}\text{Ne}, ^{20}\text{Ne})^{16}\text{O}$ elastic scattering at $E_{c.m.} = 24.5$, 24.7, and 27.9 MeV. The dashed black curves denote pure optical model fits to the data for angles $\theta_{c.m.} < 90^\circ$. The solid red curves denote the results of DWBA calculations including the $^{16}\text{O}(^{20}\text{Ne}, ^{16}\text{O})^{20}\text{Ne}$ elastic transfer process. The shaded red area on the $E_{c.m.} = 24.7$ MeV plot indicates the spread due to the uncertainty in C^2S given in Table II. Note that data sets at different energies have been displaced by successive factors of 10^{-3} for the sake of clarity.

B. DWBA calculations of elastic transfer

By confining the optical model fits to the $^{16}\text{O}(^{20}\text{Ne}, ^{20}\text{Ne})^{16}\text{O}$ elastic scattering data to angles $\theta_{c.m.} < 90^\circ$, effects due to the $^{16}\text{O}(^{20}\text{Ne}, ^{16}\text{O})^{20}\text{Ne}$ elastic transfer and other processes such as inelastic scattering should be excluded from the resulting angular distributions. We take the elastic transfer explicitly into account to first order by means of DWBA calculations. The DWBA amplitude for the $^{16}\text{O}(^{20}\text{Ne}, ^{16}\text{O})^{20}\text{Ne}$ transfer process $f_{\text{DWBA}}(\pi - \theta)$ is added to the optical model elastic scattering amplitude $f_{\text{el}}(\theta)$.

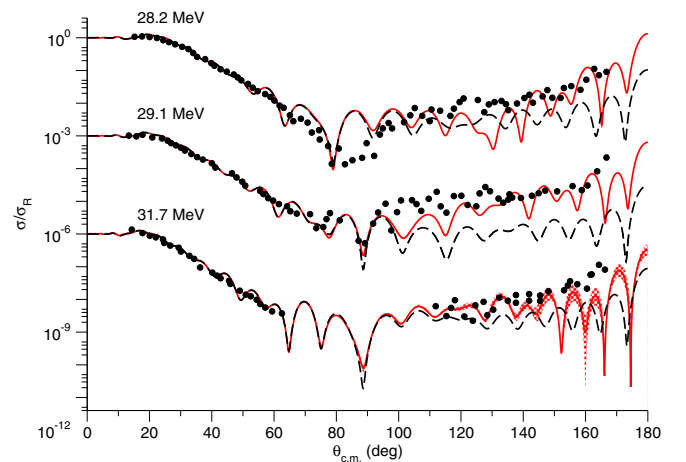


FIG. 2. Same as Fig. 1 but for energies $E_{c.m.} = 28.2$, 29.1, and 31.7 MeV. The shaded red area on the $E_{c.m.} = 31.7$ MeV plot indicates the spread due to the uncertainty in C^2S given in Table II. Note that data sets at different energies have been displaced by successive factors of 10^{-3} for the sake of clarity.

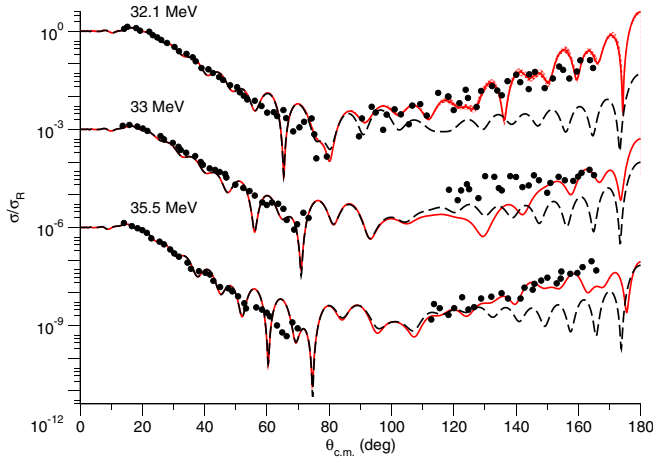


FIG. 3. Same as Fig. 1 but for energies $E_{c.m.} = 32.1, 33,$ and 35.5 MeV. The shaded red area on the $E_{c.m.} = 32.1$ MeV plot indicates the spread due to the uncertainty in C^2S given in Table II. Note that data sets at different energies have been displaced by successive factors of 10^{-3} for the sake of clarity.

Due to the particular nature of the elastic transfer process the DWBA calculations only require the following inputs: a $^{20}\text{Ne} + ^{16}\text{O}$ optical model potential, a $^4\text{He} + ^{16}\text{O}$ binding potential, and a spectroscopic factor, C^2S , for the $\langle ^{20}\text{Ne} | \alpha + ^{16}\text{O} \rangle$ overlap. The number of nodes in the $^4\text{He} + ^{16}\text{O}$ radial wave function is fixed by the Talmi-Moshinsky relation [18], as in Ref. [12], and gives $N = 5$ for a relative $^4\text{He} + ^{16}\text{O}$ angular momentum $L = 0$, counting the node at $r = 0$ but not that at $r = \infty$. We fix the optical model potential for a given incident energy at that obtained in the optical model fits and the parameters of the $^4\text{He} + ^{16}\text{O}$ binding potential are fixed at the same values [12] as those used to calculate the CF potential. The DWBA calculations therefore have a single adjustable parameter at each energy, the spectroscopic factor for the $\langle ^{20}\text{Ne} | \alpha + ^{16}\text{O} \rangle$ overlap.

Best fit values of C^2S were obtained by minimizing χ^2/N , this time over the whole angular range, and the results are given in Table II in the rows labeled “DWBA.” The quoted uncertainties were obtained by grid searches on C^2S around the best fit value and represent the spread given by a 10% increase of χ^2/N away from the minimum value. The DWBA fits to the elastic scattering data are denoted in Figs. 1–3 by the solid red curves. The spread in the backward angle cross sections due to the uncertainties in C^2S given in Table II is indicated on the figures for three representative data sets by the red shading. The gross structures of the backward hemisphere angular distributions are reasonably well described, particularly the magnitude, although detailed fits are not obtained; given the relatively simple nature of the calculations detailed fits are not expected. Test CRC calculations confirmed that DWBA is adequate to describe the direct one-step elastic transfer since they gave identical results to those plotted in Figs. 1–3.

The error-weighted mean value obtained for the $^{20}\text{Ne} \rightarrow \alpha + ^{16}\text{O}$ spectroscopic factor in this work is $C^2S = 0.54 \pm 0.03$. The individual determinations are plotted in Fig. 4 which also displays the mean value (horizontal solid line) and its error band (grey shading).

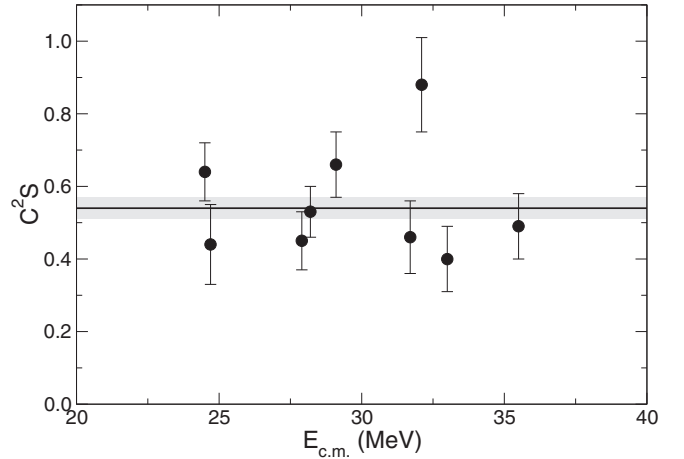


FIG. 4. The values of C^2S extracted from the DWBA calculations as a function of $E_{c.m.}$. The horizontal solid line denotes the error-weighted mean value with its error band (grey shading).

III. DISCUSSION

Measured angular distributions for the $^{16}\text{O}(^{20}\text{Ne}, ^{20}\text{Ne})^{16}\text{O}$ elastic scattering at nine different energies have been satisfactorily described by a combination of optical model fits based on CF model potentials and DWBA calculations explicitly including the $^{16}\text{O}(^{20}\text{Ne}, ^{16}\text{O})^{20}\text{Ne}$ elastic transfer process; see Figs. 1–3. The CF procedure provides a convenient way to produce consistent optical potentials based on a $^{16}\text{O} + \alpha$ cluster picture of ^{20}Ne . The pure optical model calculations are able satisfactorily to fit the data for angles $\theta_{c.m.} < 90^\circ$ using these potentials with normalization factors very close to unity for both the real and imaginary parts at all the energies studied. In Fig. 5 we plot the volume integrals of the best fit potentials as a function of energy. There is a certain amount of scatter

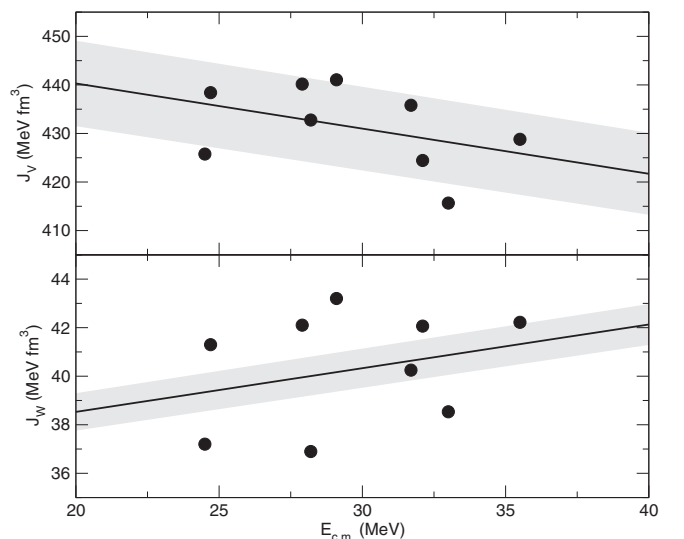


FIG. 5. Volume integrals per nucleon pair for the best fit optical potentials as a function of energy. The solid curves denote straight line regression fits. The grey shading represents uncertainty bands of $\pm 2\%$.

in the values but the general trends are for reducing J_V and increasing J_W as a function of energy, as shown by the solid lines which are straight line regression fits. The values and trends are in reasonable agreement with those for neighboring systems [19]. These results, together with the best fit N_R and N_I values—close to 1.0 and only weakly dependent on energy—support the use of the Watanabe-type cluster folding model as a means for producing consistent optical potentials on which to base a DWBA analysis of the elastic transfer.

Using these potentials as input to the DWBA calculations and fixing the $\alpha + ^{16}\text{O}$ binding potential to be the same as that used in calculating the CF potentials so as to be completely self-consistent, the only adjustable parameter in the calculations was the spectroscopic factor for the $(^{20}\text{Ne} | ^{16}\text{O} + \alpha)$ overlap, which was searched on to obtain the best fit to the backward angle data. With this procedure we obtained consistent spectroscopic factors from all the data sets analyzed, with the exception of the $E_{c.m.} = 32.1$ MeV set which yields an anomalously high value; see Table II and Fig. 4. This suggests either the presence of a resonance in the ^{36}Ar compound system at the corresponding excitation energy or the extra enhancement of the backward angle cross section due to the inability of the system to absorb the higher partial waves at this particular energy, as discussed by Eberhard [20] in the context of anomalous large-angle scattering of α particles. However, Miao *et al.* [21] report statistically significant correlated structures at $E_{c.m.} = 23.0, 25.8,$ and 29.0 MeV in excitation functions for several channels in the $^{20}\text{Ne} + ^{16}\text{O}$ partition which they associate with resonances in ^{36}Ar , but none at $E_{c.m.} = 32.1$ MeV. Conversely, the spectroscopic factor obtained at $E_{c.m.} = 29.1$ MeV, while somewhat larger than the mean is not anomalously so. This suggests that the large spectroscopic factor obtained at $E_{c.m.} = 32.1$ MeV is most likely ascribable to angular momentum dependent absorption effects similar to those described by Eberhard [20].

If we discard the value obtained at $E_{c.m.} = 32.1$ MeV the error-weighted mean $C^2S = 0.52 \pm 0.03$, not significantly different from that extracted from the full data set. It should be emphasized that the quoted uncertainties apply only to the set of choices we have made in our analysis; other choices, particularly of the $\alpha + ^{16}\text{O}$ binding potential, could lead to substantially different values. Nevertheless, the value obtained is self-consistent and the small variation of the individual values obtained from the different data sets provides considerable *a posteriori* justification of the analysis. To give some indication of the sensitivity of the extracted C^2S values to the distorting potentials, we repeated the exercise with the N_R and N_I values of the CF potentials held fixed at unity. The resulting C^2S values agreed with those given in Table II within the stated uncertainties, with the exception of that obtained from the $E_{c.m.} = 33$ MeV data which was significantly higher (0.71 ± 0.12). The error-weighted mean C^2S is 0.60 ± 0.03 , or 0.59 ± 0.03 if the $E_{c.m.} = 32.1$ MeV value is discarded, both in good agreement with the values obtained when N_R and N_I are tuned to give the optimum fit to the forward angle elastic scattering data.

Comparison of spectroscopic factors from different analyses is always problematic, mainly due to the well-known dependence of the absolute values obtained on the choice

of binding potential parameters. It is particularly difficult in the case of α spectroscopic factors since the absolute values obtained often vary considerably depending on the particular α -particle transfer reaction employed and, for a given reaction, the incident energy of the projectile, even when similar α -particle binding potentials are used. Consequently often only relative α spectroscopic factors are quoted in the literature, since any comparison of empirical values will only be meaningful if the same (or very similar) α -cluster binding potential has been used in the different determinations. Comparison with theoretical values has a different set of problems, since theoretical and empirical spectroscopic factors are not strictly speaking the same quantities, the latter being in essence the normalization factor required to match an angular distribution calculated with some reaction theory to the corresponding measured one.

With this in mind we do not attempt an exhaustive comparison with previous values for the $(^{20}\text{Ne} | ^{16}\text{O} + \alpha)$ spectroscopic factor, merely citing some representative examples. The study of the $^{20}\text{Ne}(p, p\alpha)$ reaction at 101.5 MeV by Carey *et al.* [22] gives two values for the spectroscopic factor, determined using a standard Woods-Saxon $\alpha + ^{16}\text{O}$ binding potential and one calculated by folding an α -nucleon interaction into the core density. These are 0.54 ± 0.08 and 0.64 , respectively, the quoted uncertainty on the value obtained with the Woods-Saxon binding potential corresponding to the errors on the experimental data. In this instance a comparison of the Woods-Saxon value with that obtained in this work, 0.52 ± 0.03 , is meaningful since the radius and diffuseness parameters, $R = 1.3 \times 16^{1/3}$ fm and $a = 0.65$ fm, yield an $\alpha + ^{16}\text{O}$ relative wave function almost identical to that used here. The most recent theoretical calculation of the $(^{20}\text{Ne} | ^{16}\text{O} + \alpha)$ spectroscopic factor [23] gives a value of 0.755, although there is a considerable range of values given by other formalisms, e.g., 0.448 [24] and 0.229 [25]. While comparisons between experimentally derived and theoretically calculated spectroscopic factors are at best subjective, the value obtained in this work is at least reasonable in comparison with the results of these calculations. Comparison with the empirical value of Ref. [22] is more straightforward, since although the reactions concerned are very different both spectroscopic factors are obtained by normalizing theoretical cross sections to measured ones. Since the $\alpha + ^{16}\text{O}$ relative wave functions in both cases are almost identical the excellent agreement between the two values is physically meaningful, providing further support for the consistent approach adopted in this work.

IV. CONCLUSIONS

In this work we have presented a consistent analysis of the $^{16}\text{O}(^{20}\text{Ne}, ^{20}\text{Ne})^{16}\text{O}$ elastic scattering at nine energies, explicitly including the $^{16}\text{O}(^{20}\text{Ne}, ^{16}\text{O})^{20}\text{Ne}$ elastic transfer process via the DWBA. In this way it was possible to extract a self-consistent value for the $(^{20}\text{Ne} | ^{16}\text{O} + \alpha)$ spectroscopic factor of 0.52 ± 0.03 which was essentially energy independent. The energies studied are free of resonances in the ^{36}Ar compound nucleus [21] apart from the data at $E_{c.m.} = 29.1$ MeV which do not appear to be affected, although the data at $E_{c.m.} =$

32.1 MeV yield an anomalously large value for the spectroscopic factor, possibly connected with angular momentum dependent absorption effects similar to those discussed by Eberhard [20].

An advantage of the current approach over previous work is that it fixes both the real and imaginary parts of the distorting optical potential in a consistent way, thus quantifying the contribution of other processes to the backward angle rise in the elastic scattering data. Attempting to include explicitly two-step transfer paths would increase the number of parameters to be determined from the same data set (signs as well as magnitudes of spectroscopic amplitudes in CCBA calculations) so the further assumption was made that these paths would affect the phase of the oscillations in the backward angle cross section but not its magnitude.

Our conclusions are as follows: A consistent approach whereby the same α cluster model is used to generate the optical potentials and the potential binding the exchanged α particle to the two ^{16}O cores leads to consistent results over several different data sets. We performed two sets of analyses, one where the normalization factors of the real and imaginary

parts of the CF optical potential were varied to obtain the best description of the forward hemisphere elastic scattering data at each energy and one where they were both held fixed to unity for all data sets. Both analyses gave similar results for the $(^{20}\text{Ne} | ^{16}\text{O} + \alpha)$ spectroscopic factor. The resulting spectroscopic factor and the accompanying binding potential [12] provide a reliable $(^{20}\text{Ne} | ^{16}\text{O} + \alpha)$ overlap that could be used in α -particle transfer studies using the $(^{20}\text{Ne}, ^{16}\text{O})$ and/or $(^{16}\text{O}, ^{20}\text{Ne})$ reactions. Finally, the results of our study provide *a posteriori* validation of the $^{16}\text{O}(^{20}\text{Ne}, ^{16}\text{O})^{20}\text{Ne}$ transfer proceeding mostly as a simple one-step exchange of an α particle between the two identical cores since the DWBA theory is able to provide a satisfactory and above all consistent description of the data.

ACKNOWLEDGMENT

Sh.H. would like to thank the Heavy Ion Laboratory of the University of Warsaw for hospitality during the period in which this work was carried out.

-
- [1] R. Stock, U. Jahnke, D. L. Hendrie, J. Mahoney, C. F. Maguire, W. F. W. Schneider, D. K. Scott, and G. Wolschin, *Phys. Rev. C* **14**, 1824 (1976).
- [2] M. Gai, G. M. Berkowitz, P. Braun-Munzinger, C. M. Jachcinski, C. E. Ordoñez, T. R. Renner, and C. D. Uhlhorn, *Phys. Rev. C* **30**, 925 (1984).
- [3] Y. Kondō, B. A. Robson, and R. Smith, *Nucl. Phys. A* **410**, 289 (1983).
- [4] Y. Kondō, B. A. Robson, and R. Smith, *Nucl. Phys. A* **437**, 117 (1985).
- [5] C. Gao, Y. Kondō, and B. A. Robson, *Nucl. Phys. A* **529**, 234 (1991).
- [6] Y. Kondō, B. A. Robson, R. Smith, and H. H. Wolter, *Phys. Lett. B* **162**, 39 (1985).
- [7] C. Gao and G. He, *Phys. Lett. B* **282**, 16 (1992).
- [8] N. Burtebayev, M. Nassurulla, D. Alimov, I. Boztosun, J. Burtebayeva, A. K. Morzabayev, S. K. Sakhiev, S. V. Artemov, and J. M. Mussaev, *J. Phys.: Conf. Ser.* **590**, 012056 (2015).
- [9] Y.-X. Yang and Q.-R. Li, *Phys. Rev. C* **84**, 014602 (2011).
- [10] I. J. Thompson, *Comput. Phys. Rep.* **7**, 167 (1988).
- [11] S. Watanabe, *Nucl. Phys.* **8**, 484 (1958).
- [12] B. Buck, J. C. Johnston, A. C. Merchant, and S. M. Perez, *Phys. Rev. C* **52**, 1840 (1995).
- [13] M. P. Nicoli, F. Haas, R. M. Freeman, N. Aissaoui, C. Beck, A. Elanique, R. Nouicer, A. Morsad, S. Szilner, Z. Basrak, M. E. Brandan, and G. R. Satchler, *Phys. Rev. C* **60**, 064608 (1999).
- [14] J. M. Cervera, A. Garcia, and F. Senent, *An. Fis. Quim.* **64**, 33 (1968).
- [15] G. R. Satchler and W. G. Love, *Phys. Rep.* **55**, 183 (1979).
- [16] D. T. Khoa and W. von Oertzen, *Phys. Lett. B* **342**, 6 (1995).
- [17] S. Qing-biao, F. Da-chun, and Z. Yi-zhang, *Phys. Rev. C* **43**, 2773 (1991).
- [18] I. Talmi, *Helv. Phys. Acta* **25**, 185 (1952).
- [19] M. E. Brandan and G. R. Satchler, *Phys. Rep.* **285**, 143 (1997), and references therein.
- [20] K. A. Eberhard, *Phys. Lett. B* **33**, 343 (1970).
- [21] Y. Miao, R. W. Zurmühle, S. P. Barrow, N. G. Wimer, J. T. Murgatroyd, C. Lee, and Z. Liu, *Phys. Rev. C* **53**, 815 (1996).
- [22] T. A. Carey, P. G. Roos, N. S. Chant, A. Nadasen, and H. L. Chen, *Phys. Rev. C* **29**, 1273 (1984).
- [23] A. Volya and Y. M. Tchuvil'sky, *Phys. Rev. C* **91**, 044319 (2015).
- [24] J. Hiura, F. Nemoto, and H. Bandō, *Prog. Theor. Phys. Suppl.* **52**, 173 (1972).
- [25] K. Katō and H. Bandō, *Prog. Theor. Phys.* **59**, 774 (1978).